Volume 1 | Number 1 | Jan 2013 | Pages 1–100

Dalton Transactions

An international journal of inorganic chemistry
www.rsc.org/dalton

ROYAL SOCIETY OF CHEMISTRY

ROYAL SOCIETY OF CHEMISTRY

www.rsc.org/dalton

Journal Name

ARTICLE

Tuning the target composition of amine-grafted CPO-27-Mg for capture of CO_2 in post-combustion and air filtering conditions: a combined experimental and computational study

M. C. Bernini[*a], A.A. García Blanco[b], J. Villarroel-Rocha[b], D. Fairen-Jimenez[c], K. Sapag[b], A. J. Ramirez-Pastor[b] and G. E. Narda[a]

A computational and experimental screening of hypothetical and real compounds exhibiting different degree of ethylenediamine grafted to the CPO-27-Mg or Mg-DOBDC skeleton is performed in order to determine the target composition that optimizes the CO_2 adsorption properties in flue gas and air filtering conditions. On the basis of the $[Mg_2(dobdc)]$ formula, eighteen hypothetical models involving 15-100% of functionalization of the coordinatively unsaturated sites (CUS) were considered by means of Grand Canonical Monte Carlo simulations to evaluate the CO_2 adsorption at 298 K. In addition, post-synthesis modification was applied to CPO-27-Mg leading to three kinds of samples exhibiting 15, 50, 60 % of CUS functionalization with ethylenediamine, named CPO-27-Mg-a, CPO-27-Mg-b and CPO-27-Mg-c. Compounds were characterized using elemental analysis, TGA, FTIR spectroscopy, PXRD and DSC. Finally, bare and functionalized CPO-27-Mg materials were evaluated using gas adsorption and microcalorimetry in the 0.001-1 bar range, which is the pertinent for the mentioned applications. Valuable information related to design criteria for synthesis of tuned CO_2 adsorbents is derived through this computational and experimental investigation.

1. INTRODUCTION

Facing the global warming concern, technologies involving CO_2 capture can be performed in pre-combustion, post-combustion or in oxy-combustion routes. Since the operating conditions vary greatly with each method, the required features of materials in each process are also different.[1] An interesting alternative involves the selective removal of CO_2 from gas mixtures by the carbon capture and sequestration (CCS) processes, which includes the compression of pure CO_2 to a supercritical fluid, the transportation to an injection site, and finally its destination to an underwater or underground storage.[2] A critical step in these technologies is the selective separation of CO_2 from the gas mixtures that integrate the different gas flows in each chemical process.

The elimination of CO_2 from low pressure flue gases as emitted, for example, by fossil fuel burning power plants can be accomplished very effectively by means of gas scrubbing.[3] The partial pressure of CO_2 in these streams lies between 50-200 mbar.[1,4,5] Aqueous amine solutions (e.g. monoethanol amine) are currently being used as absorbents for the removal of CO_2 from industrial commodities, a technique which has been employed in the natural gas industry for more than 60 years.[6] However, this methodology has several disadvantages such as pipe corrosion, high energy consumption associated with the regeneration of the absorbent solution, degradation in the presence of oxygen and SO_x, etc. As such, the use of solid adsorbents, which are easy to regenerate and exhibit a high affinity for selective CO_2 adsorption in flue gas conditions, has been proposed as a good alternative for CO_2 capture in thermal plants.[7] Additionally, carbon dioxide scrubbers are critical to life support systems in confined spaces with limited air exchange, such as spacecrafts, submarines, and re-breathing suits.[8] With these applications in mind, research into the direct capture of this gas from more diluted stream gases is also underway, being studied for its implementation in air filter technologies, with 5 mbar serving as a reference pressure value.[9] Zeolites[10], activated carbons[11], silicas[12], and new classes of porous materials[13] have been investigated for their CO_2 adsorption behaviour. Among them, MOFs with high porosity, good thermal stability and containing strong Lewis acid-basic sites are emerging as one of the most promising candidates and have demonstrated excellent qualities for

a Área de Química General e Inorgánica, Facultad de Química, Bioquímica y Farmacia, Universidad Nacional de San Luis. Instituto de InvestigacionesenTecnologíaQuímica (INTEQUI-CONICET).5700 San Luis. Argentina. E-mail:mcbernin@unsl.edu.ar
b Departamento de Física. Universidad Nacional de San Luis. Instituto de FísicaAplicada (INFAP-CONICET).5700 San Luis. Argentina
c Department of Chemical Engineering and Biotechnology, University of Cambridge,Pembroke St., Cambridge CB2 3RA, UK.

separation of multicomponent systems, such as CO_2–N_2 and CO_2–CH_4.[14]

Experimental and theoretical investigations have shown that CPO-27-M[15], where M is a divalent metal, is a particularly promising material.[16] This MOF (also known as M-MOF-74[17] or M-DOBDC[15-f]) consists of one dimensional channels completely lined with coordinatively unsaturated sites (CUS), and it can be synthesized with Mg, Mn, Fe, Co, Ni, Cu, and Zn as the metal center. The enthalpy of adsorption ($\Delta_{ads}h$) of CO_2 in these materials at low loadings has been reported in the range of 37-73 kJ·mol^{-1} [15-a,f,18,19] and such particular large enthalpy values have been associated with the interaction of CO_2 with the CUS in the structure. For post-combustion capture, the desired range of $\Delta_{ads}h$ lies between the physisorption and chemisorption energies, which would be optimal for the regenerability of a material having sufficient CO_2 specificity to be economically viable.[20] A reliable determination of this parameter is then desirable in order to characterize the adsorbate-adsorbent interaction and to critically evaluate the applicability of these kinds of materials. In general, this parameter is derived from isotherm data obtained at two or, less frequently, three temperatures, applying the Clausius-Clapeyron equation. Only few studies have involved the direct measurement of $\Delta_{ads}\dot{h}$ of CO_2 in MOFs by adsorption microcalorimetry, and even less examples in the case of amine-functionalized MOFs.[21] The CPO-27-M family is also important because expanded versions of these MOF have been synthesized using longer DOBDC linker analogues, conducing to materials with extremely high porosity.[22] Additionally, the CUS are suitable for post-synthetic modification, allowing the incorporation of further polar functional groups that may increase the chemical affinity with specific adsorbates, which is desirable for capture of CO_2 from diluted (post-combustion) and very diluted (enriched environments) stream gases. In particular, the grafting of diamine molecules on CUS, has demonstrated improvement in CO_2 adsorption performance.[23]

In recent papers, one degree of functionalization of CUS was studied experimentally by grafting diamine molecules in the CPO–27-M members[24,25] and expanded analogues[9,26] for CO_2 adsorption applications. Thus, 25% of CUS present in CPO-27-Ni were functionalized by anchoring a cyclic diamine (piperazine), showing a good CO_2/N_2 adsorption selectivity, but without improving the adsorption capacity at low pressure, when compared to the non-functionalized material. Considering the analogue CPO-27-Mg[15-g], about 11.11% of the CUS were functionalized by using ethylenediamine, showing an increased adsorption capacity at ultradilute gas stream conditions (p_{CO_2} = 0.0004 bar, equivalent to 400 ppm of CO_2 in a N_2 gas flow) in comparison with the bare material.[25] The Mg_2(dobpdc) compound, adopting an isoreticular expanded CPO-27 structure (1)[26], was also modified by the functionalization of 80% of its CUS employing ethylenediamine (1-en)[26] and N,N'-dimethylethylenediamine (mmen-Mg_2(dobpdc))[9], exhibiting promising features for CO_2 adsorption from flue gas mixtures and from air in ambient conditions. Moreover, these functionalized Mg_2(dobpdc)

compounds showed higher stability than the non-functionalized analogous when exposed to atmospheric conditions.[9]

Taking this into account, we decided to perform a screening of a high number of real and hypothetical materials with different degrees of ethylenediamine functionalization. We carried out CO_2 adsorption experiments on three fully characterized samples exhibiting 15-60% of CUS functionalization. Besides, eighteen hypothetical models were considered for complementary Monte Carlo simulations, covering 15-100% of CUS functionalization. This procedure aims to determine the targeted composition that optimizes selective CO_2 capture for flue gas and air filtration technologies, through a systematic variation of ethylenediamine incorporation in the CPO-27-Mg skeleton. The incidence of the incorporated -NH_2 groups/free CUS-Mg^{2+} ratio, the pore geometry, the pore size distribution (PSD) and the remaining void volume fraction in the CO_2 adsorption performance and CO_2/N_2 selectivity is analysed. Moreover, once the best composition of amine-grafting was identified, recycling experiments and determination of differential enthalpy of adsorption from direct microcalorimetry measurements of both functionalized and non-functionalized versions of CPO-27-Mg were carried out.

2. Experimental Section

2.1 Synthesis of CPO-27-Mg

This compound was obtained following a reported procedure,[15-f] in which 1.83 mmol of $Mg(NO_3)_2$·$6H_2O$ and 0.53 mmol of 2,5-dihydroxyterephthalic acid were dissolved in a mixture of solvents composed by 44 mL of dimethylformamide (DMF), 3 mL of ethanol and 3 mL of distilled water. The resultant solution was heated at 398 K for 21 h in a Teflon-lined digestion Parr bomb (120 mL of internal volume). After that, the reactor was immediately cooled to room temperature and the yellow microcrystalline powder obtained was filtered and washed with DMF and methanol. The solid was left in contact with methanol (50 mL) and it was replaced four times over three days. Finally, the solvent was extracted with a Pasteur pipette and the solid was dried at room temperature.

2.2 Post-synthetic modification of CPO-27-Mg with ethylendiamine

Samples of CPO-27-Mg were thermally treated in dynamic vacuum conditions in order to remove the solvent (coordinated and non-coordinated). The resulting partially activated samples were put in contact with different solutions of ethylenediamine in toluene, with the aim of obtaining materials with different amine-grafted content. The suspensions were stirred for 65 h at room temperature, after which the solid was separated by centrifugation and washed with toluene and hexane. The samples obtained by this procedure were dried at 333 K for 2 h. The details of the functionalization procedures of each sample (named as CPO-27-Mg-a, CPO-27-Mg-b and CPO-27-Mg-c) are displayed in the Electronic Supporting Information, ESI.

The content of amine grafted was studied by ATG-DSC, FTIR and elemental analysis; see Figures S1-S3 and Table S1, ESI. Powder X-ray Diffraction allowed confirming the structure and stability of all products (see Figure S4, ESI).

All samples, non-functionalized and functionalized, were employed in adsorption experiments and characterizations within 24 h of their preparation. During this time all samples were kept under ambient conditions.

2.3 Powder X-Ray Diffraction (PXRD)

PXRD patterns were obtained with a Rigaku D-MAX-IIIC diffractometer using Cu Kα radiation (λ=1.5418 Å) and quartz as external calibration standard. The best counting statistics were achieved using a scanning step of 0.03° between 4° and 50° Bragg angles with an exposure time of 5 s per step.

2.4 Fourier-Transform Infrared Spectroscopy (FTIR)

FTIR spectra were recorded with a Nicolet Protégé 460 spectrometer in the 4000–225 cm^{-1} range with 64 scans and a spectral resolution of 4 cm^{-1} using the KBr pellet technique.

2.5 Thermal Analysis

Thermogravimetric Analysis (TGA) and Differential Scanning Calorimetry (DSC) were performed between room temperature and 873 K, employing a Shimadzu TGA-51 and a DSC-60 apparatus, respectively, under air flowing at 50 mL min^{-1}, and a heating rate of 10 K min^{-1}.

2.6 Elemental Analysis

Elemental analyses for C, H and N were conducted in an Exeter CE 440 instrument. The samples were analyzed both as-prepared and after activation processes (performed for recording adsorption isotherms) without additional thermal treatment. The proposed stoichiometries for each sample are shown in Table S1, ESI.

2.7 Gas Adsorption

Before the measurement of the adsorption isotherms, the CPO-27-Mg samples were degassed at 523 K (or 503 K in the case of ethylenediamine grafted samples) during 6 h in dynamic vacuum (20 µTorr). The most convenient outgassing temperature for the functionalized samples was determined by considering the TG-DSC curves of CPO-27-Mg-c (See Figures S1 and S2, ESI).

Measurements of N$_2$ (99.999%) at 77 K were carried out using a manometric adsorption equipment (ASAP 2000, Micromeritics). The Brunauer, Emmett and Teller (BET) method[27] applied to N$_2$ adsorption data was used to estimate the specific surface area (S$_{BET}$) of the samples, where the consistency criteria proposed by Rouquerol et al.[28] were taken into account. CO$_2$ (99.995% purity) adsorption isotherms were measured in a manometric adsorption apparatus (Micromeritics, ASAP 2050) at 298 and 323 K.

In order to evaluate the reusability of the functionalized and non-functionalized CPO-27-Mg samples, two consecutive CO$_2$ adsorption isotherms at 298 K were obtained, and to evaluate the stability of the porosity of both materials under the recycling conditions, an equivalent experiment was performed by adsorbing N$_2$ at 77 K in two consecutive cycles. Experimental details are described in Section S7, Supporting

Information. All of these experiments were carried out in a manometric adsorption apparatus (Micromeritics, ASAP 2050).

2.8 CO$_2$ Adsorption Microcalorimetry

CO$_2$ adsorption microcalorimetric experiments were performed at room temperature (~300 K) using ~0.07 g of sample. The evolved heat was measured using a Tian-Calvet microcalorimeter (model CA-100, ITI), which was connected to an adsorption manometric setup to measure simultaneously the adsorption isotherm and the differential enthalpy of adsorption. A pressure transducer of 1000 Torr that provides high accuracy and high resolution in the 3·10^{-5} to 1.4 bar range was employed.

The total heat (Q) produced in each adsorption step was calculated as:

$$Q = K \int_{t_0}^{t_1} E_V \, dt, \quad (1)$$

where E_V is the voltage signal (in V) registered between times t_0 and t_1 and K is the microcalorimeter constant (in W·V^{-1}), determined by electrical calibrations. The so-called discontinuous procedure was used, where the differential enthalpy of adsorption ($\Delta \dot{h}_{ads\,T,n}$) is given by[28]:

$$\Delta \dot{h}_{ads\,T,n} = \left(\frac{dQ_{rev}}{dn^\sigma} \right)_T + V_C \cdot \left(\frac{dp}{dn^\sigma} \right)_T, \quad (2)$$

where dQ_{rev} is the heat reversibly exchanged with the surroundings at temperature T, dn$^\sigma$ is the adsorbed amount due to the pressure increase dp and V_C is the dead volume of the adsorption cell immersed in the microcalorimeter. According to the setting of the instrument, and since the magnitude of the second term of Eq. (2) is negligible with respect to the first one, the differential enthalpy of adsorption ($\Delta \dot{h}_{ads\,T,n}$) was calculated by using:

$$\Delta \dot{h}_{ads\,T,n} = \left(\frac{dQ_{rev}}{dn^\sigma} \right)_T \quad (3)$$

It is important to remark that the enthalpy of CO$_2$ adsorption is frequently expressed as the isosteric heat of adsorption (Q$_{st}$) as a function of the quantity of CO$_2$ adsorbed.[1] The Q$_{st}$ value is a parameter that describes the average enthalpy of adsorption for an adsorbing gas molecule at a specific surface coverage and is usually evaluated using two or more CO$_2$ adsorption isotherms collected at similar temperatures (usually within 10 K of each other). However, even though the term Q$_{st}$ is now discouraged and should be replaced by the isosteric enthalpy of adsorption[28], it is still frequently found in related literature.

3. Computational Details

3.1 Models of CPO-27-Mg with ethylenediamine grafted

Three initial conformations for the ethylenediamine molecule adopting three different N-C-C-N dihedral angle (ω) were considered, i.e. i) ω$_1$ = 60°, ii) ω$_2$ = -60° and iii) ω$_3$ = 180°. For each one, six different models were obtained by grafting these

ethylenediamine molecules into 1 to 6 inorganic chains (SBUs, secondary building units) of the framework's hexagonal channels. Each model is denoted as $\omega_{i\text{-}J}$, where i = 1-3, depending on the ethylenediamine dihedral angle, and J = 1-6, depending on the degree of functionalization. The unit cells of each model were then subjected to energy minimization and geometry optimization based on molecular mechanics, which include van der Waals and electrostatic interactions, allowing for modification of unit cell size and the atomic coordinates of the new structures. These calculations were performed with the Forcite module of Materials Studio, using an algorithm which is a cascade of the steepest descent, an adjusted basis Newton-Raphson set, and quasi-Newton methods.[29] The bonded and the short range (van der Waals) interactions between atoms were modeled using the Universal Force Field (UFF).[30] A cut-off distance of 18.5 Å was used for the van der Waals interactions during the geometry optimization. The long-range, electrostatic interactions, arising from the presence of partial atomic charges, were modelled using a Coulombic term. The Ewald sum method was used to compute electrostatic interactions. Partial atomic charges were derived using the charge equilibration method (QEq) as implemented in Materials Studio.[31]

3.2 Monte Carlo Simulations

The CO_2 adsorption at 298 K was studied using grand canonical Monte Carlo (GCMC) simulations, performed with the multi-purpose code RASPA.[32] Atomistic models obtained as described above were used as adsorbent models. Framework atoms were kept fixed at their crystallographic positions in all simulations. CO_2-CO_2 and CO_2-framework interactions were calculated using a Lennard-Jones (LJ) + Coulomb potential. LJ parameters for the C, H and O atoms of the CPO-27 skeleton were taken from the Dreiding[33] force field and the ones corresponding to the Mg atom were taken from the UFF[32]; those parameters corresponding to C, H and N atoms belonging to the ethylenediamine portion were taken from the TraPPE force field[34] developed for amine molecules (see Table S2, Section S8 in ESI). Carbon dioxide was modeled as a linear triatomic molecule with fixed bond lengths and bond angles. The atoms were modeled by charged Lennard-Jones (LJ) centers using the TraPPE force field developed by Potoff and Siepmann (see Table S3).[35] This force field has been fit to reproduce the vapour-liquid coexistence curves. Lorentz-Berthelot mixing rules were used for all cross terms, and LJ interactions beyond 12.8 Å were neglected. Coulomb interactions were calculated using partial charges on the atoms, calculated by the QEq method as described above. The Ewald sum method was used to compute the electrostatic interactions. Up to 4×10^4 Monte Carlo equilibration cycles were performed plus 4×10^4 production cycles to calculate the ensemble averages. In one cycle, N moves were performed, where N is the number of molecules in the system (which fluctuates in GCMC). Monte Carlo moves used with equal probability were translation, rotation, insertion, deletion and random reinsertion of an existing molecule at a new position. The pore volume was obtained using a Widom particle

insertion method, by probing the structure with a helium molecule at room temperature, and recording a large number of random points not overlapping the van der Waals volume of the framework.[36] The pore size distributions were calculated using the method of Gelb and Gubbins[37], where the largest sphere that can fit in a random point within a structure, without overlapping the van der Waals surface of the framework, is recorded for a large number of random points.

4. Results and Discussion

4.1 Post-synthesis modification and characterizations

Three samples exhibiting different ethylenediamine content after post-synthesis modification were obtained and fully characterized. Elemental analysis of %C, %H and %N were conducted for all functionalized samples before and after the adsorption experiments (see Table S1, Supporting Information). Because the as-synthesized samples and the samples used in the adsorption studies were kept under standard atmospheric conditions, and since the elemental analysis was conducted in air, CO_2 was present in some samples. This was also observed in the expanded CPO-27-Mg analogue compound functionalized with ethylenediamine[26]. According to the elemental analysis, the formulae of the post-synthetic functionalized samples are $[Mg_2(DHT)(H_2O)_{1.7}(en)_{0.3}]\cdot5H_2O$ (as-synthesized CPO-27-Mg-a), $[Mg_2(DHT)(H_2O)(en)]\cdot0.2(en)\cdot3H_2O$ (as-synthesized CPO-27-Mg-b) and $[Mg_2(DHT)(H_2O)_{0.8}(en)_{1.2}]\cdot0.2(en)\cdot3H_2O$ (as-synthesized CPO-27-Mg-c). Thus, we were able to prepare samples exhibiting CUS functionalization degrees of 15, 50 and 60 %, respectively.

Thermogravimetric analysis was also conducted for all samples, so that the proposed formulae from elemental analysis could be confirmed (see Figure S1, ESI). Differential scanning calorimetry (DSC) was performed in order to evaluate the energy variation as a function of thermal treatment (see Figure S2, ESI). A detailed description of the TGA-DSC curves is displayed in Section S3 of ESI.

The incorporation of ethylenediamine in the CPO-27-Mg frameworks was also studied qualitatively by FTIR spectroscopy. As can be seen in Figures 1 and S3, several new bands coincident with those of ethylenediamine appear in the IR spectra of the functionalized samples.

Those bands located at ~3350, 3290 and 3175 cm^{-1} are suitable for the assignment to N-H stretching vibrations, while those at ~ 2930 and 2865 cm^{-1} are assigned to the stretching of aliphatic C-H bonds. Moreover, two bands located at ~1000 and 965 cm^{-1} in the spectra of those samples exhibiting higher amine content can be associated with the same vibration of aliphatic C-C bonds. Interestingly, the bands located at 407, 374 and 331 cm^{-1} in the spectrum of the CPO-27-Mg compound are shifted to 399, 367 and 316 cm^{-1} in the corresponding spectra of the functionalized analogues which exhibited higher amine contents (CPO-27-Mg-b and -c). This could be associated with the elongation of the Mg-O bonds in the MgO$_5$ polyhedra consequential from the activation-

followed by the grafting of ethylenediamine process. Furthermore, two weak bands at ~303 and 290 cm^{-1} can be assigned to Mg-N stretching vibration, and as can be seen in Figure 6 and S3, they are more notorious in the spectrum of CPO-27-Mg-c, in keeping with the highest amount of amine present in this compound.
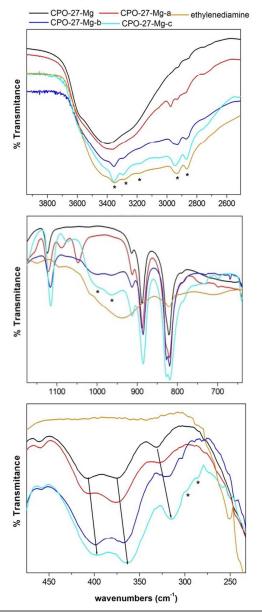

Figure 1. FTIR spectra of as synthesized CPO-27-Mg, CPO-27-Mg-a, -b and -c and ethylenediamine in selected spectral zones. The bands marked with * are assigned to ethylenediamine molecules.

4.2 CO_2 adsorption isotherms

The most convenient outgassing temperature was determined analysing the TG-DSC curves, looking for the optimal temperature at which the non-coordinated ethylenediamine and the eventual solvent molecules remaining at the framework channels were evacuated, without eliminating the coordinated ethylendiamine ones. As an example, Figure S5 shows the effect of different outgassing temperatures in the CO_2 adsorption performance of CPO-27-Mg-c sample. When it is outgassed at 393 K in dynamic vacuum, the CO_2 adsorption capacity is low, showing that the pores remain mostly blocked, but at an outgassing temperature of 503 K, the CO_2 adsorption capacity is strongly increased. Thus, 503 K was selected as the outgassing temperature for all functionalized samples, while 523 K was chosen for the non-functionalized one.

In order to properly correlate the adsorption performance with the ethylenediamine composition, the elemental analysis of all samples was studied at the end of the adsorption experiments. Thus, the amine content measured corresponds to the one kept after the outgassing procedure performed before adsorption. The corresponding formulae for the recovered samples are $[Mg_2(DHT)(H_2O)_{1.7}(en)_{0.3}]\cdot 3H_2O$ (CPO-27-Mg-a), $[Mg_2(DHT)(H_2O)_{1.2}(en)_{0.8}]\cdot 0.4CO_2\cdot 4H_2O$ (CPO-27-Mg-b) and $[Mg_2(DHT)(H_2O)(en)]\cdot CO_2\cdot 2H_2O$ (CPO-27-Mg-c), which represent 15%, 40% and 50% of functionalization remaining after the outgassing treatment. The difference between the amine contents, of the as-synthesized and post-isotherm samples, is due to the outgassing treatment, which includes heating in dynamic vacuum conditions.

The CO_2 adsorption isotherms measured at 298 K for the four samples under study are displayed in Figure 2. The amounts adsorbed at key pressure values are presented in Table 1 along with the corresponding values obtained for other functionalized CPO-27 compounds[9,24,26] for the sake of comparison.

At ~1 bar the adsorption capacity of the CPO-27-Mg is about 7.1 $mmol\cdot g^{-1}$, which is slightly lower than the highest reported value (8.1 $mmol\cdot g^{-1}$) for this MOF[38], being the difference probably related to the storage and manipulation conditions applied (vacuum in ref. 38 or atmospheric conditions in this work). The adsorption capacities for the functionalized samples at ~1 bar decrease to 5.22, 4.97 and 5.42 $mmol\cdot g^{-1}$, for CPO-27-Mg-a, -b, and -c, respectively. The decrease of about 25-30% could be associated with the reduction of the free void fraction in the ethylenediamine-containing samples. A similar behaviour was observed for the CPO-27-Ni and piperazine-CPO-27-Ni compounds[24] with the corresponding adsorption capacities at this pressure being ~5.5 $mmol\cdot g^{-1}$ and 3.2 $mmol\cdot g^{-1}$, respectively. It is interesting to note that even when the functionalization degree of Ni-CUS was only 25%, the influence of employing the bulkier diamine molecule piperazine is evident in the more marked uptake decrease, being about 42 % less than the corresponding value for the non-functionalized compound.

As a consequence of the incorporation of polar functional groups into the pore, the adsorbent-adsorbate interactions were modified, affecting the adsorption performance, particularly at low pressures (below 0.2-0.3 bar). For this reason, it is interesting to analyse carefully the impact of the different functionalization degrees on the adsorption isotherms focusing in two key pressure zones: 5 mbar (important for air filtering technologies), and 50-200 mbar (for capture in post-combustion conditions).
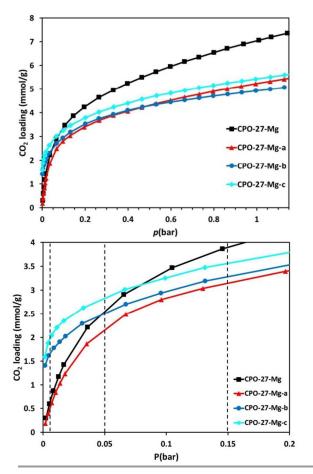
Figure 2. Experimental CO_2 adsorption isotherms obtained for CPO-27-Mg and functionalized CPO-27-Mg samples at 298 K.Dashed

4.2.1 CO_2 capture in the 5-50 mbar pressure range

In this pressure range, different adsorption behaviour is observed for the functionalized samples relative to the non-functionalized material. As shown in Figure 2, the isotherm of the sample containing 15% functionalized CUS (CPO-27-Mg-a) is below the corresponding one to the non-functionalized material over this pressure range, showing that this degree of amine content does not improve CO_2 affinity compared to the CPO-27-Mg compound. A similar situation is also observed for the CPO-27-Ni and the piperazine-grafted compound, since the adsorption capacity of the functionalized adsorbent is lower than that of the non-functionalized one.[24] The opposite is true for those samples with 40% (CPO-27-Mg-b) and 50% (CPO-27-Mg-c) CUS functionalization, which exhibit a higher CO_2 adsorption up to 50 mbar and 65 mbar, respectively, relative to the performance of the CPO-27-Mg. Interestingly, the best performance in this pressure range is exhibited by the sample containing 50% of the Mg^{2+} CUS grafted with ethylenediamine molecules (CPO-27-Mg-c). At 5 mbar, a reference pressure value for CO_2-enriched environments[8], this material adsorbs 2 mmol·g^{-1}, which is 3.3 times higher than the amount adsorbed by the non-functionalized one. This value is close to the one reported for mmen-Mg_2(dobpdc)[9] (2.6 mmol·g^{-1}), and

significantly smaller than the reported value for 1-en[26] (3.3 mmol·g^{-1}). Samples with more than 50% of amine functionalization remaining after the outgassing process could not be obtained, since the maximum achieved functionalization degree was 60%, which might be a limit value related with the pore volume availability. Additionally, according to A. Das et al.[20] primary amines like ethylenediamine, exhibit a high tendency to form hydrogen bond interactions among them, reducing the possibility to effectively coordinate the CUS in the MOF framework, precluding the availability of higher degrees of post synthesis modification in microporous systems. However, considering our results, it would be of interest to perform a screening of a wide range of functionalization degree to some of the IRMOF-74[22] members, since eight out of nine of those materials exhibit pore diameters in the range of mesopores (> 20 Å).

4.2.1 CO_2 capture in the 50-150 mbar pressure range

At 150 mbar, which is a reference value for the partial pressure of CO_2 in flue gas conditions, CPO-27-c adsorbs 3.6 mmol·g^{-1}, which is the same amount reported for 1-en[26] and slightly more than the amount adsorbed by mmen-Mg_2(dobpdc)[9] (see Table 1). Considering the different performances found for the functionalized samples with respect to the bare material, and taking into account the operative conditions of the flue gas in industrial facilities, CO_2 adsorption isotherms were also measured at 323 K for CPO-27-Mg and CPO-27-Mg-c (see Figure 3). At this temperature, the presence of diamine grafted molecules improves the CO_2 adsorption below 65 mbar of pressure compared to the non-functionalized material, while at 150 mbar the adsorption capacity of CPO-27-Mg is 20% higher than that of CPO-27-Mg-c.

These results suggest that the latter material could be more efficient in those applications that require a high chemical affinity to selectively adsorb CO_2 in the presence of other components (e.g., in air filter technologies).
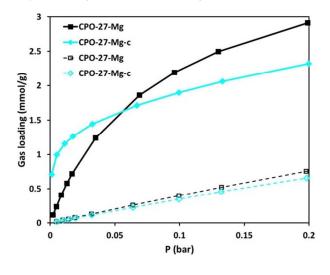

Figure 3. CO_2 (filled symbols) and N_2 (open symbols) adsorption isotherms obtained at 323 K for the CPO-27-Mg and CPO-27-Mg-c samples.

Table 1. Experimental CO_2 adsorption loadings obtained in this study and related compounds

Sample	% of functionalized CUS	Uptake at 5 mbar (mmol·g^{-1})	Uptake at 50 mbar (mmol·g^{-1})	Uptake at 150 mbar (mmol·g^{-1})	Uptake at 1 bar (mmol·g^{-1})	Reference
CPO-27-Mg	0	0.6	2.55	3.9	7.1	This work
CPO-27-Mg-a	15	0.5	2.20	3.12	5.22	This work
CPO-27-Mg-b	40	1.6	2.48	3.25	4.92	This work
CPO-27-Mg-c	50	2	2.85	3.6	5.42	This work
CPO-27-Mg	0	-	5	6.1	8.1	38
CPO-27-Ni	0	-	1.5	3.3	5.4	24
pip-CPO-27-Ni	25	-	0.8	1.25	3.2	24
1	0	-	-	-	-	26
1-en	80	3.3	3.45	3.62	4.57	26
Mg$_2$(dobpdc)	0		3.8	4.85	6.42	9
mmen-Mg$_2$(dobpdc)	80	2.6	2.9	3.13	3.86	9

Moreover, considering the significant reduction of the specific surface area and the micropore volume by the functionalization treatment, i.e. S_{BET} = 1280 m^2·g^{-1} and V_o-DR = 0.49 cm^3·g^{-1} for the bare material to S_{BET} = 400 m^2·g^{-1} and V_o-DR = 0.16 cm^3·g^{-1} for CPO-27-Mg-c sample (see Figure S6 in ESI), it is remarkable the impact of introducing polar functional groups leading to an optimum composition and porous architecture that increase notably the CO_2 adsorption at low pressure.

In order to deepen into the characterization of the sample whose composition seems to be optimal, and since the main component of air and flue gases is N_2, the adsorption isotherms of this gas were also measured at 323 K for both, CPO-27-Mg and CPO-27-Mg-c. As shown in Figure 3, N_2 loading below 65 mbar is lower than 0.22 mmol·g^{-1}, and at 5 mbar it is 0.0165 mmol·g^{-1}. The corresponding CO_2 loadings at this pressure for CPO-27-Mg and CPO-27-Mg-c were 0.24 and 1 mmol·g^{-1}, respectively. This shows the considerable improvement that may incorporate this particular functionalization degree in the CO_2 selectivity.

4.3 Recycling experiments and differential enthalpy of adsorption of CO_2

In order to complete the characterization of CO_2 adsorption for the optimal composition (50% of CUS functionalization), and to properly evaluate the reusability of this material in comparison with that of the non-functionalized one, two consecutive CO_2 adsorption isotherms were performed at 298 K, including an outgassing step between both experiments (see experimental details, section 2.8). As seen in Figure 4, the adsorption capacity of the CPO-27-Mg-c suffers an important decrease in the second cycle, while the performance of the non-functionalized material remains almost unaltered.

This result could be due to: i) a possible alteration of the porous architecture (partial degradation) by the whole recycling process; ii) the permanence of some CO_2 molecules "strongly" adsorbed on the CPO-27-Mg-c MOF surface that would block the strongest adsorption sites and fill partially the porosity, diminishing the available pore volume and

consequently, give rise to a lower adsorption capacity along the whole pressure range.
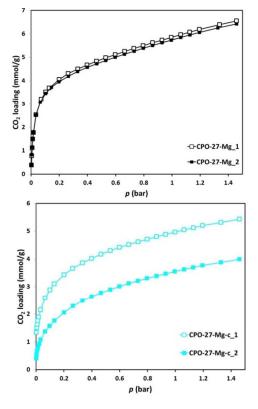

Figure 4. CO_2 recycling experiments performed at 298 K for CPO-27-Mg (up) and CPO-27-Mg-c (down); 1 and 2 denote the first and second cycle, respectively.

In order to investigate the hypothesis stated in i) an analogue recycling experiment employing the functionalized and bare materials was performed by means of N_2 adsorption at 77 K. If the porous architecture of any material is affected by the recycling process, a diminution in the second N_2 adsorption isotherm should be appreciated. However, Figure 5 shows that

only for the case of the non-functionalized compound a small diminution during the second cycle is observed, but both isotherms of the CPO-27-Mg-c are almost coincident, thus indicating that the porosity is not affected by the recycling procedure. These results suggest that CO_2 molecules have a strong interaction with the framework surface of CPO-27-Mg-c, since in spite of the outgassing treatment between the isotherms (at 503 K during 6 hours in dynamic vacuum conditions), the pores of the functionalized sample would be partially filled with CO_2 at the beginning of the second cycle.

are shown in Figure 6, while the associated adsorption isotherms are displayed in Figure S7.

As can be seen, the differential enthalpy of adsorption at ~ zero loading is highly incremented in the case of the functionalized CPO-27-Mg-c material, being the initial value of 132 kJ mol^{-1} associated with a chemisorption process. In the case of the bare CPO-27-Mg material, this magnitude reaches the value of 53 kJ mol^{-1}, which is close to the maximum values found for this MOF by applying the Clausius-Clapeyron determination method.[1]

Figure 6. Differential enthalpy of adsorption of CO_2 vs. loading determined by microcalorimetry experiments for CPO-27-Mg and CPO-27-Mg-c at ~300 K.

According to our measurements, the adsorption-desorption process involved in the case of the functionalized compound is not completely reversible, since different magnitudes of energy (as heat) were measured during the adsorption and desorption steps, being higher in the case of the adsorption one. This fact suggests that part of the CO_2 adsorbed molecules is strongly chemisorbed and, thus, they remain within the framework. Regarding the magnitude of the measured enthalpy and the observed non-reversibility of the process, the formation of a stable carbamate species could be occurring. This fact justifies the decrease in the second cycle of the CO_2 adsorption isotherm and suggests that in spite of the selectivity being highly improved with the targeted composition, stronger energetic requirements may be needed to remove all the CO_2 adsorbed molecules, which is not desirable for technological applications. In contrast, under the applied conditions (adsorption of pure CO_2 gas) the non-functionalized material showed a reversible behaviour with a measured differential enthalpy of adsorption at ~ zero loading being about 53 kJ·mol^{-1}. This was determined not only by getting the same energy magnitudes on the adsorption and desorption processes, but also by keeping the same adsorption capacity during the second cycle (see Figure 4). However, as it was already shown,[39] the adsorption capacity of the non-functionalized CPO-27-Mg material is strongly diminished by the presence of water in the post-combustion gases mixture.
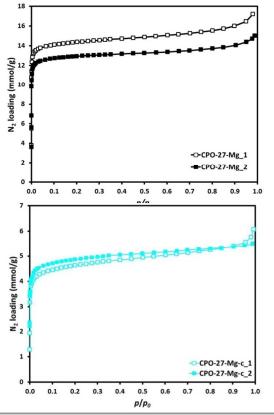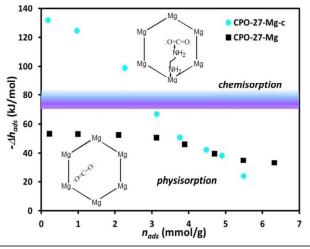

Figure 5. N_2 adsorption recycling experiments performed at 77 K for CPO-27-Mg (up) and CPO-27-Mg-c (down); 1 and 2 denote the first and second cycle, respectively.

It follows that a reliable determination of the differential enthalpy of adsorption in both materials is of great importance, since this value is directly related to the chemical affinity between the adsorbent and the adsorbate and may justify the selectivity as well as energy requirements for releasing CO_2 molecules during the regeneration process. Using an adsorbent that binds CO_2 too strongly would increase the regeneration cost due to the energy required to break the framework-CO_2 interactions. Meanwhile, if the enthalpy of adsorption is too low, the material could be more readily regenerated, but the purity of the captured CO_2 would be lowered due to the decreased adsorption selectivity.[1]

The differential enthalpy of adsorption of CO_2 as a function of loading was determined as a direct measurement by microcalorimetry experiments and the corresponding profiles
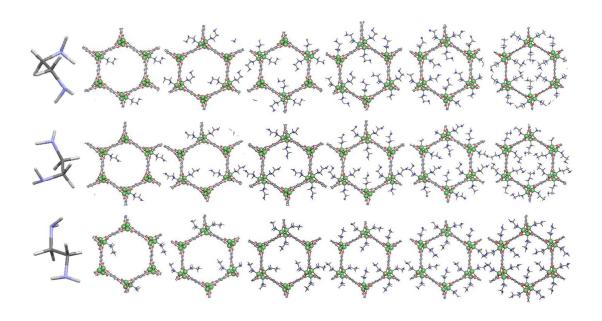
Journal Name

ARTICLE

Figure 7. Models of CPO-27-Mg exhibiting different degrees of ethylenediamine grafted molecules, ω_1-J (top); ω_2-J (middle) and ω_3-J (bottom) models. The initial conformations of the diamine molecules is also shown (left) for each set of models.

4.4 Molecular simulations

In order to deeply understand the results obtained for the functionalized materials and, since no samples exhibiting more than 60% of CUS functionalization were obtained experimentally, we decided to perform a complementary molecular simulation study. To this aim, three sets of six hypothetical models of ethylenediamine-grafted CPO-27-Mg structures were obtained by functionalizing different proportions of CUS in the original MOF. This involved the functionalization of 16.6, 33.3, 50, 66.6, 83.3 and 100% of CUS (see Figure 7). The void fraction varies from ~0.64 to ~0.13 (non-porous) for the 16.6% to 100% of functionalization in each of the three sets of models (see Table 2). When studying the geometry of the grafted ethylenediamine molecules, it can be observed that those models coming from the initial gauche conformations (ω_1-J and ω_2-J) are energetically more stable than those obtained by the initial extended or trans ones (ω_3-J). The ω_2-J structures are in turn the most stable ones for all the functionalization degrees (see Table 2).

Table 2. Functionalization degrees, void fractions, and potential energy values for the ω_i-J models obtained after energy minimization.

Model	% Functionalization	Void Fraction	Energy (kJ mol^{-1})
ω_1-1	16.6	0.640	-29844.36
ω_1-2	33.3	0.566	-30002.448
ω_1-3	50	0.448	-30051.21
ω_1-4	66.6	0.356	-29992.284
ω_1-5	83.3	0.274	-30061.458
ω_1-6	100	Non-porous	-8754.606
ω_2-1	16.6	0.640	-30744.546
ω_2-2	33.3	0.544	-30890.244
ω_2-3	50	0.443	-30888.48
ω_2-4	66.6	0.350	-30524.508
ω_2-5	83.3	0.272	-30193.422
ω_2-6	100	Non-porous	-8881.404
ω_3-1	16.6	0.642	-29410.626
ω_3-2	33.3	0.543	-29176.644
ω_3-3	50	0.442	-28606.284
ω_3-4	66.6	0.327	-28486.248
ω_3-5	83.3	0.199	-28262.346
ω_3-6	100	Non-porous	-7854.126

ARTICLE

Journal Name

Figure 8. Simulated CO_2 adsorption isotherms for: ω_1-J (top); ω_2-J (middle) and ω_3-J (bottom) models.

It is interesting to mention the marked diminution in the magnitude of the energy associated to the ω_i-6 models, which reflects the strong steric impediments resultant form the saturation of 100 % of CUS with the ethylenediamine molecules. From a conformational point of view, it seems that the geometry adopted by ethylenediamine molecules confined inside the pores and grafted to the CUS is governed by the "gauche effect".[40] The corresponding values of the dihedral angles for the ethylenediamine grafted molecules after the energy minimization procedure are displayed in Table S4, ESI.

The simulated PSDs of the three sets of models (Figure S8) are quite similar for all structures; however as can be seen in Figures S9 and S10, the shape of the pores is equivalent only for the ω_i-1 models, while the porous architectures show clear differences between ω_i-2 and ω_i-6, being more notable for the ω_i-3 structures. Differences in pore geometry can induce different adsorption behaviours in porous materials[41], which is expected for the ω_i-J systems, with i = 1-3 and J = 2-5.

Simulations of CO_2 adsorption isotherms at 298 K were performed for the eighteen hypothetical structures and also for the non-functionalized CPO-27-Mg (see Figure 8). The simulated isotherm obtained for the original material is similar to that reported by A. O. Yazaydin et al.[15-e]. Simulations in MOFs containing open metal sites[15-e,42] give rise to underestimation of adsorption at low pressure when compare to the experimental isotherms, which accounts for deficiencies in the employed generic force fields that do not properly represent the strong interaction between the adsorbate molecules and CUS. This situation was indeed observed when comparing our simulated and experimental isotherms. However, as the same force field is employed for all systems under study, it is appropriate to compare the simulated adsorption performance among all models, to investigate the existence of trends as functions of the different degrees of functionalization.

Since the CO_2 molecule has a quadrupole moment in which the carbon atom is polarized positively and the oxygen ones are polarized negatively, the adsorbate-adsorbent interactions can include both atoms of the CO_2 molecule and different parts of the MOF skeleton (i.e., OCO:➔Mg or H_2N:➔CO_2). Thus, the first one involves the non-functionalized part of the framework while the second one is dependent on the incorporation and proper localization (the real availability) of the $-NH_2$ groups of the ethylenediamine grafted molecules. Considering this, and taking into account the observed tendencies in the experiments, there are two possibilities. On one hand, could be better to functionalize the majority of the available CUS in the structure to improve the chemical adsorbent-adsorbate attraction? On the other hand, is there a particular composition of free CUS/functionalized CUS, having a singular pore sub-structure that can effectively optimize the adsorption properties? In this scenario it is important to highlight that the increase in the functionalization degree is accompanied by a diminution in the void pore volume and, as such, both factors play a key role in the adsorption process.

As it is seen in Figure 8 the incorporation of the amine groups in the pore surface affects the adsorbent-adsorbate interactions and modifies the adsorption performance at low pressure (below 0.2-0.3 bar). The comparison of the isotherms of the ω_i-J systems in this pressure range shows that the adsorption capacity exhibits a complex dependence on the chemical composition, pore shape and available pore volume.

The most remarkable fact is the evidence that the adsorption is not regulated by free void volume in all systems under study, since different behaviors are observed for systems with almost equal available pore volume (see Table 2). Thus, for the ω_1-J and ω_2-J models, there is a tendency to increase the

adsorption up to those containing 33.3% (ω_1-2) or 50% (ω_2-3) functionalization, with a consequent diminution when the degree of functionalization is further elevated. On the contrary, the adsorption in the ω_3-J systems seems to be modulated by the void fraction since the adsorption capacity decreases along with the diminution of the available pore volume when the functionalization degree increases. This finding suggests that the shape of the pore is of great importance to the resulting adsorption performance.

An interesting fact is observed if we focus on the ω_2-J systems (Figure 8-middle), which were the most stable models for all degrees of functionalization. In the low pressure zone, a tendency in the adsorption capacity as ω_2-1 <ω_2-2 <ω_2-3 is evident. Moreover, the simulated capacity for the ω_2-3 model is higher than that simulated for the non-functionalized CPO-27-Mg MOF, both at ~5 mbar and 150 mbar, the key pressure values for CO_2 capture in spacecraft cabins and flue-gas, respectively. This fact suggests that the 50% functionalization of CUS in the CPO-27 structure could represent an optimized composition and porous architecture, which may improve the performance of CO_2 adsorption for flue gas mixtures and for air purification applications. Here, we highlight that, to the best of our knowledge, there are no studies of CO_2 adsorption either in any CPO-27-M or in the expanded analogous versions that exhibit this particular degree of functionalization.

On the basis of the PSD (Figure S8) pore shape images (Figures S9 and S10), and simulated isotherms (Figure 8), the CO_2 adsorption seems to be highly favoured by the formation of a sub-structure of regular cylindrical pores of ~ 5 Å in diameter, in which there is a 1/1 ratio of free Mg-CUS/available $-NH_2$ groups, that is achieved for the 50% of CUS functionalization.

Linking both, experimental and computational results, and considering the available data on the related CPO-27-M or M-MOF-74 family and on the diamine-functionalized versions, design criteria to obtain optimized CO_2 adsorbents arise. On one hand, it seems a reasonable possibility that applying the target composition of 50% of CUS functionalization to a CPO-27-M member based on a lower attractive metal ion could give rise to reduce the differential enthalpy of adsorption and thus, the energy regeneration requirements. For example, CPO-27-Co was found having the lowest enthalpy of adsorption (37 kJ·mol^{-1} [15-f]) and also was found as the most stable one under the humidity conditions of the flue gas mixtures.[39] On the other hand, if the optimal functionalization degree is applied to an extended CPO-27-Co compound based on a longer dicarboxylate linker (i.e. a mesoporous member of the IRMOF-74 series), the increase in framework channel size and void volume can lead to an incremented adsorption capacity along with a lower adsorbent-adsorbate interaction, helping to further reduce the differential enthalpy of adsorption and obtaining a good equilibrium between selectivity and regeneration costs.

5. Conclusions

By combining experiments and simulations, a screening of real and hypothetical materials exhibiting different degrees of CUS

functionalization in CPO-27-Mg structure was performed to identify the optimum features of CO_2 adsorbent materials for air filtering and flue-gas applications. According to experimental and simulated CO_2 adsorption isotherms, recycling studies and microcalorimetry measurements, the functionalization degree involving 50% of CUS could be a tuned composition for CO_2 adsorption in flue gas and air filter technologies. However, considering the associated high regeneration energy cost, we suggest that an optimized adsorbent having the expanded CPO-27 structure based on a weaker Lewis acid metal ion, would allow modulating adsorbate-adsorbent interactions as a strategy to overcome the energy requirements for the regenerability step.

Acknowledgements

Notes and references

1 K. Sumida, D. L. Rogow, J. A. Mason, T. M. McDonald, E. D. Bloch, Z. R. Herm, T. Hyun Bae, J. R. Long *Chem. Rev.* **2012**, 112, 724–781.

2 DOE/NETL Carbon Dioxide Capture and Storage RD&D Roadmap; National Energy Technology Laboratory, 2010.

3 a) H. Q. Yang, Z. H. Xu, M. H. Fan, R. Gupta, R. B. Slimane, A. E. Bland, I. Wright *J. Environ. Sci.* **2008**, 20, 14-27; b) R. Carapellucci, A. Milazzo *Proc. Inst. Mech. Eng. Part A.* **2003**, 217, 505-517.

4 A. U. Czaja, N. Trukhan, U. Müller *Chem. Soc. Rev.* **2009**, 38, 1284–1293.

5 a) D. M. D'Alessandro, B. Smit, J. R. Long *Angew. Chem., Int. Ed.* **2010**, 49, 6058-6082; b) Q. Wang, J. Luo, Z. Zhong, A. Borgna *Energy Environ. Sci.* **2011**, 4, 42-55.

6 G. T. Rochelle *Science* **2009**, 325, 1652-1654.

7 R. S. Haszeldine *Science* **2009**, 325, 1647–1652.

8 a) H. W. Carhart, J. K. Thompson *ACS Symposium Series* 17; American Chemical Society: Washington, DC, 1975; p 1; b) P. O. Wieland Controlling Carbon Dioxide. Living Together in Space: The Design and Operation of the Life Support Systems on the International Space Station; NASA/TM-98-206956/VOL1; NASA Marshall Space Flight Center: Marshall Space Flight Center, AL, 1998; Chapter 3.3.1, p 121.

9 T. M. McDonald, W.R. Lee, J. A. Mason, B.M. Wiers, C. S. Hong, J. R. Long *J. Am. Chem. Soc.* **2012**, 134, 7056–7065.

10 Y. Lee, D. Liu, D. Seoung, Z. Liu, C. C. Kao, T. Vogt *J. Am. Chem. Soc.* **2011**, 133, 1674-1677.

11 G. P. Hao, W. C. Li, D. Qian, G. H. Wang, W. P. Zhang, T. Zhang, A. Q. Wang, F. Schüth, H. J. Bongard, A. H. Lu *J. Am. Chem. Soc.* **2011**, 133, 11378-11388.

12 A. Sayari, Y. Belmabkhout *J. Am. Chem. Soc.* **2010**, 132, 6312 –6314.

13 a) B. Wang, A. P. Côté, H. Furukawa, M. O'Keeffe, O. M. Yaghi *Nature* **2008**, 453, 207-211; b) C. Sarah, F. M. D. Joeri, V. B. Gino, R. Tom, G. Jorge, K. Freek *J. Am. Chem. Soc.* **2009**, 131, 6326-6327; c) K. L. Kauffman, J. T. Cuip, A. J. Allen, L. Espinal, W. Wong-Ng, T. D. Brown, A. Goodman, M. P. Bernardo, R. J.

Pancoast, D. Chirdon, C. Matranga *Angew. Chem., Int. Ed.* **2011**, 50, 10888-10892.

14 a) J. R. Li, R. J. Kuppler, H. C. Zhou *Chem. Soc. Rev.* **2009**, 38, 1477-1504; b) J. Zhang, H. Wu, T. J. Emge, J. Li *Chem. Commun.* **2010**, 46, 9152-9154.

15 a) D. Britt, D. Tranchemontagne, O. M. Yaghi *Proc. Natl. Acad. Sci. U. S. A.* **2008**, 105, 11623–11627; b) P. D. C. Dietzel, V. Besikiotis, R. Blom *J. Mater. Chem.* **2009**, 19, 7362–7370; c) L. Valenzano, B. Civalleri, S. Chavan, G. T. Palomino, C. Arean, S. Bordiga *J. Phys. Chem. C* **2010**, 114, 11185–11191; d) H. Wu, J. M. Simmons, G. Srinivas, W. Zhou, T. Yildirim *J. Phys. Chem. Lett.* **2010**, 1, 1946–1951; e) A. O. Yazaydin, R. Q. Snurr, T. H. Park, K. Koh, J. Liu, M. D. LeVan, A. I. Benin, P. Jakubczak, M. Lanuza, D. B. Galloway, J. J. Low, R. R. Willis *J. Am. Chem. Soc.* **2009**, 131, 18198–18199; f) S. R. Caskey, A. G. Wong-Foy, A. J. Matzger *J. Am. Chem. Soc.* **2008**, 130, 10870–10871; g) E. D. Bloch, L. J. Murray, W. L. Queen, S. Chavan, S. N. Maximoff, J. P. Bigi, R. Krishna, V. K. Peterson, F. Grandjean, G. J. Long, B. Smit, S. Bordiga, C. M. Brown, J. R. Long *J. Am. Chem. Soc.* **2011**, 133, 14814–14822, h) P. D. C. Dietzel, R. Blom, H. Fjellvag, *Eur. J. Inorg. Chem.* **2008**, 23, 3624-3632.

16 Y.-S. Bae, R. Q. Snurr *Angew. Chem. Int. Ed.* **2011**, 50, 11586–11596.

17 N. L. Rosi, J. Kim, M. Eddaoudi, B. L. Chen, M. OKeeffe, O. M. Yaghi *J. Am. Chem. Soc.* **2005**, 127, 1504-1518.

18 Z. B. Bao, L. A. Yu, Q. L. Ren, X. Y. Lu, S. G. Deng *J. Colloid Interface Sci.* **2011**, 353, 549–556.

19 J. A. Mason, K. Sumida, Z. R. Herm, R. Krishna, J. R. Long *Energy Environ. Sci.* **2011**, 4, 3030–3040.

20 A. Das, D. M. D'Alessandro *CrystEngComm.* **2015**, 17, 706-718.

21 S. V. Vaesen, Q. Guillerm, A. D. Yang, B. Wiersum, B. Marszalek, A. Gil, M. Vimont, T. Daturi, P. L. Devic, P. Llewellyn, C. Serre, G. Maurin, G. De Weireld. *Chem. Commun.* **2013**, 49, 10082-10084.

22 H. Deng, S. Grunder, K. E. Cordova, C. Valente, H. Furukawa, M. Hmadeh, F. Gándara, A. C. Whalley, Z. Liu, S. Asahina, H. Kazumori, M. O'Keeffe, O. Terasaki, J. F. Stoddart, O. M. Yaghi *Science* **2012**, 336,1018-1023.

23 a) T. M. McDonald, D. M. D'Alessandro, R. Krishna, J. R. Long *Chem. Sci.* **2011**, 2, 2022-2028; b) Q. Yan, Y. Lin, C. Kong, L. Chen *Chem. Commun.* **2013**, 49, 6873-6875.

24 A. Das, P. D. Southon, M. Zhao, C. J. Kepert, A. T. Harris, D. M. D'Alessandro *Dalton Trans.* **2012**, 41, 11739-11744.

25 S. Choi, T. Watanabe, T.-H. Bae, D. Sholl, C. W. Jones *J. Phys. Chem. Lett.* **2012**, 3, 1136-1141.

26 W. R. Lee, S. Y. Hwang, D. W. Ryu, K. S. Lim, S. S. Han, D. Moon, J. Choide, C. S. Hong *Energy Environ. Sci.* **2014**, 7, 744.

27 S. Brunauer, P.H. Emmett, E. Teller *J. Am. Chem. Soc.* **1938**, 60, 309-319.

28 F. Rouquerol, J. Rouquerol, K.S.W. Sing, P. Llewellyn, G. Maurin Adsorption by powders and porous solids: Principles, methodology and applications. Academic Press, San Diego, CA, U.S.A, 2014.

29 a) D. Fairen-Jimenez, Y. J. Colón, O. K. Farha, Y.-S. Bae, J. T. Hupp, R. Q. Snurr. *Chem. Commun.* **2012**,48, 10496-10498; b) N. L. Strutt, D. Fairen-Jimenez, J. Iehl, M. B. Lalonde, R. Q. Snurr, O. K. Farha, J. T. Hupp, J. F. Stoddart *J. Am. Chem. Soc.* **2012**, 134 (42),17436–17439; c) W. Bury, D. Fairen-Jimenez, M. B. Lalonde, R. Q. Snurr, O. K. Farha, J. T. Hupp *Chem. Mater.* **2013**, 25 (5), 739–744.

30 A. K. Rappe, C. J. Casewit, K. S. Colwell, W. A. Goddard, W. M. Skiff *J. Am. Chem. Soc.* **1992**, 114, 10024-10035.

31 Materials Studio v6.1. Accelrys Software Inc., San Diego, CA 92121, USA.

32 D. Dubbeldam, S. Calero, D. E. Ellis, R. Q. Snurr *Mol. Sim.* **2015**, 1-21.

33 S. L. Mayo, B. D. Olafson, W. A. Goddard III *J. Phys. Chem.* **1990**, 94, 8897-8909.

34 C. D. Wick, J. M. Stubbs, N. Rai, J.I. Siepmann *J. Phys. Chem. B* **2005**, 109, 18974-18982.

35 a) J. J. Potoff, J. I. Siepmann *AlChE J.* **2001**, 47, 1676-1682; b) M. G. Martin, J. I. Siepmann *J. Phys. Chem.B* **1998**, 102, 2569.

36 a) M. Arif Nadeem, A. W. Thornton, M. R. Hill, J. A. Stride *Dalton Trans.* **2011**, 40, 3398-3401; b) R. Krishna, J. M. van Baten *Phys. Chem. Chem. Phys.* **2011**, 13, 10593-10616; c) T. Duren, F. Millange, G. Ferey, K. S. Walton, R. Q. Snurr *J. Phys. Chem. C* **2007**, 111, 15350-15356; e) A. L. Myers ed. T. M. Letcher, Royal Society of Chemistry, Cambridge, 2004.

37 L. D. Gelb, K. E. Gubbins *Langmuir* **1998**, 15, 305–308.

38 D. Yu, A. O. Yazaydin, J. R. Lane, P. D. C. Dietzel, R. Q. Snurr *Chem. Sci.* **2013**, 4, 3544–3556.

39 A. C. Kizzie, A. G. Wong-Foy, A. J. Matzger *Langmuir* **2011**, 27, 6368–6373.

40 a) E. Juaristi, ''Introduction to Stereochemistry and Conformational Analysis,'' Wiley & Sons, New York, 1991, chap. 18; b) E. Juaristi, G. Cuevas ''The Anomeric Effect,'' CRC Press, Boca Raton, FL, 1995, chap. 4; c) Y. Sasanuma, K. Sugita *Polymer J.* **2006**, 38(9), 983–988; d) C. Aleman, J. Puiggalí*J. Org. Chem.* **1997**, 62, 3076-3080; b) D.J. Price, J.D. Roberts, W.L. Jorgensen *J. Am. Chem. Soc.* **1998**, 120, 9672-9679; e) M. C. Bernini, E. V. Brusau, J. C. Garro, G. Narda, E. L. Varetti *J. Molec. Struct.* **2008**, 888, 113-123.

41 A. I. Skoulidas, D. S. Sholl *J. Phys. Chem. A* **2003**, 107, 10132-10141.

42 J. Getzschmann, I. Senkovska, D. Wallacher, M. Tovar, D. Fairen-Jimenez, T. Duren, J. M. van Baten, R. Krishna, S. Kaskel *Microp. Mesop. Mater.* **2010**, 136/1-3, 50-58.

Table of Contents

A computational and experimental study is performed to determine the optimal composition that enhances the adsorption performance at low pressure.